



Enhanced Concanavalin A Binding to Preorganized Mannose Nanoarrays in Glycodendrimersomes Revealed Multivalent Interactions

Nina Yu. Kostina⁺, Dominik Söder⁺, Tamás Haraszti, Qi Xiao, Khosrow Rahimi, Benjamin E. Partridge, Michael L. Klein, Virgil Percec,^{*} and Cesar Rodriguez-Emmenegger^{*}

Abstract: The effect of the two-dimensional glycan display on glycan-lectin recognition remains poorly understood despite the importance of these interactions in a plethora of cellular processes, in (patho)physiology, as well as its potential for advanced therapeutics. Faced with this challenge we utilized glycodendrimersomes, a type of synthetic vesicles whose membrane mimics the surface of a cell and offers a means to probe the carbohydrate biological activity. These single-component vesicles were formed by the self-assembly of sequence-defined mannose-Janus dendrimers, which serve as surrogates for glycolipids. Using atomic force microscopy and molecular modeling we demonstrated that even mannose, a monosaccharide, was capable of organizing the sugar moieties into periodic nanoarrays without the need of the formation of liquid-ordered phases as assumed necessary for rafts. Kinetics studies of Concanavalin A binding revealed that those nanoarrays resulted in a new effective ligand yielding a ten-fold increase in the kinetic and thermodynamic constant of association.

Introduction

The glycocalyx is an information-dense array of glycolipids and glycoproteins at the cellular membranes in all

domains of life.^[1] It represents the outermost interface of the cell and thus it is the first component to interact with the environment enabling cell communication, cargo trafficking, signal transduction, tight junctions, as well as cell adhesion and interactions with the extracellular matrix.^[2] It also plays a central role in lipid and protein sorting, cell shape transformation, division, as well as embryonic development and the development of immunity.^[3] The glycan moieties at the cellular membrane are organized in unique molecular patterns that define “self” but this specific spatial arrangement can be exploited by some pathogenic bacteria and viruses to attack cells.^[4]

The immense complexity of functions of the cellular glycocalyx arises from the combination of the chemical diversity of sugar moieties and their spatial 3D presentation that provides a structural basis for controlling the affinity in sugar-protein recognition.^[4b] The spatial presentation is achieved by the lateral non-random assembly of lipids and glycolipids into nano- and microorganized domains.^[2] For this, nature exploits the preferential association of certain lipids via their hydrophilic head groups due to complementarity of molecular shapes, head groups rotational entropy, charge repulsion, and dipolar interactions, leading to nanodomains and even nanoarrays.^[5]

Not surprisingly, the importance of the glycocalyx has spawned intense research aiming at elucidating how function emerges from the spatial presentation of supramolecular arrays of glycans at the cell membrane.^[1,3,4b,6] But despite decades of work, the structure of the glycocalyx in cells remains difficult to resolve due to the limited toolkit of imaging methods even with the advances in non-linear ultra-high-resolution microscopies.^[7] Thus, various cell membrane models based on liposomes and polymersomes decorated with glycans have been developed in an effort to dissect structure-function relations.^[1,3,6a–c,8] The most advanced models aim at recapitulating a certain degree of lateral organization exploiting the coassembly of sterols with various saturated and unsaturated lipids. The strong interaction of sterols with unsaturated lipids leads to the segregation of large and stable liquid-ordered (L_o) domains.^[9] However, they display drastically different sizes, mechanical properties, and dynamics that fail to sufficiently resemble functional cell-membrane micro- and nanodomains.^[2b,10] The problem is further exacerbated when the vesicles are formed from amphiphilic block copolymers. The entanglement of the hydrophobic blocks of the polymers results in membranes with almost no lateral diffusion and are virtually frozen.^[11]

[*] Dr. N. Yu. Kostina,^[†] D. Söder,^[†] Dr. T. Haraszti, Dr. K. Rahimi, Dr. C. Rodriguez-Emmenegger
DWI- Leibniz Institute for Interactive Materials and Institute of Technical and Macromolecular Chemistry RWTH Aachen University
Forckenbeckstraße 50, 52074 Aachen (Germany)
E-mail: rodriguez@dwi.rwth-aachen.de

Dr. Q. Xiao, Dr. B. E. Partridge, Prof. Dr. V. Percec
Roy & Diana Vagelos Laboratories, Department of Chemistry,
University of Pennsylvania
Philadelphia, PA 19104-6323 (USA)
E-mail: percec@sas.upenn.edu

Dr. Q. Xiao, Prof. Dr. M. L. Klein
Institute of Computational Molecular Science, Temple University
Philadelphia, PA 19122 (USA)

[†] These authors contributed equally to this work.

Supporting information and the ORCID identification number(s) for the author(s) of this article can be found under:
 <https://doi.org/10.1002/anie.202100400>.

© 2021 The Authors. Angewandte Chemie International Edition published by Wiley-VCH GmbH. This is an open access article under the terms of the Creative Commons Attribution Non-Commercial NoDerivs License, which permits use and distribution in any medium, provided the original work is properly cited, the use is non-commercial and no modifications or adaptations are made.

Recently, Percec et al. introduced amphiphilic Janus dendrimers (JDs)^[12] and their sugar-presenting analogs, Janus glycodendrimers (JGDs),^[13] which provide synthetic alternatives to natural lipids and glycolipids. They self-assemble into cell membrane-mimics in water,^[12] named dendrimersomes (DSs) and glycodendrimersomes (GDSs).^[13,14] They display superior mechanical stability compared to lipids with energies at break close to polymersomes, while maintaining the flexibility and permeability close to the one observed on cell membranes.^[12,15] The thickness of the membrane is accurately controlled by the size and topology of the hydrophobic dendrons and can be adjusted to match the thickness of cell membranes (4–5 nm).^[12] Furthermore, DSs with more complex linear or branched oligosaccharides that mimic those in the cellular surface serve for elucidating glycan-protein interactions.^[13a,c,16] To investigate the spatial organization of these glycans at the GDSs' membranes we developed a structural analysis methodology using atomic force microscopy (AFM),^[17] fast Fourier transform (FFT) image processing, and molecular modeling.^[16a,18] We discovered that the assembly of sequence-defined JGDs on which the sugar (lactose (Lac) or oligomannose (oligo(Man))) was diluted in a defined way among tri(ethylene oxide) units in the hydrophilic dendrons gave rise to nanoarrays with the sugar moieties nanoassembled in lamellar or hexagonal patterns.^[16a,18] These periodic arrays of glycans reduced the dense packing of Lac and oligo(Man) resulting in faster agglutination in the presence of multidentate lectins.^[13c,18] But is the enhanced biological activity of the glycan just a consequence of reducing steric constraints to binding or do the nanopatterned glycans constitute more active ligands compared to the homogeneously distributed ones?

In this work, we tackle this question by quantifying the binding affinity of Concanavalin A (ConA) to GDSs decorated with nanoarrays of monosaccharide mannose (Man). Man is the simplest glycan capable of driving the formation of nanoarrays on GDSs. Similar patterns were also observed with other more complex glycans (linear and branched mannose, lactose, sulfo-lactose)^[16a,18] but Man represents a simple biomimetic model to probe our hypothesis. Furthermore, Man was selected due to its high biological relevance, in spite of not occurring as a glycolipid, as it is one of the fundamental building blocks of glycocalyx of cell membranes. The GDSs were formed by the self-assembly of sequence-defined JGDs in water. AFM analysis of GDSs' membranes allowed probing how the molecular structure controls the formation and the type of nanoarrays. Binding kinetics and the thermodynamic affinity constant were determined by monitoring the binding of ConA to the nanopatterned surfaces using surface plasmon resonance (SPR) enabling us to prove that the increase in biological activity was dictated by the formation of the nanoarray and not by steric effects.

Understanding the formation of glycan periodic nanoarrays may help to shed light on cell communication, maintenances of the characteristic composition of organelles, signaling, vesicle trafficking inside the cells, and provide a powerful example in which structure determines function, in particular how different supramolecular assemblies encode

biological recognition. Such knowledge may be of great impact in biomedicine for the development of therapeutics that distinguish between host cells and pathogens or that harness the protective functions of the immune response or therapeutic gain.^[4b,19]

Results and Discussion

Assembly of Mannose-Decorated GDSs

Onion-like GDSs were self-assembled from a library of sequence-defined JGDs prepared by an accelerated modular synthetic strategy as previously reported (Figure 1 a).^[13c] All JGDs contain methoxytriethoxy (3EO) fragments and Man as hydrophilic parts. These groups were decisive in the formation of onion-like DSs that are synthetic analogs of multivesicular bodies.^[13c,20] These JGDs share the same hydrophobic dendrons, 3,5-bis(dodecyloxy)benzoic ester, to avoid any differences in membrane flexibility and thickness stemming from the hydrophobic domains. The library includes high Man-density single-single JGD-1_{Man} and twin-twin JGD-2_{Man}, as well as JGDs in which the Man concentration is systematically reduced in the hydrophilic dendron. The sugar density was varied from 100% (JGD-1_{Man}, and JGD-2_{Man}), 3/1 3EO/Man for JGD(3/1_{Man}), 6/1 3EO/Man for JGD(6/1_{Man}), and 8/1 3EO/Man for JGD(8/1_{Man}^{2S}), JGD(8/1_{Man}^{3S}), JGD(8/1_{Man}^{2L}) and JGD(8/1_{Man}^{3L}) (Figure 1 a). Furthermore, the position of Man on the hydrophilic dendrons in the JGD 8/1 series was varied. Man was linked in the second position counted from left-to-right of the gallic amide for JGD(8/1_{Man}^{2S}) and JGD(8/1_{Man}^{2L}) and in the third position for JGD(8/1_{Man}^{3S}) and JGD(8/1_{Man}^{3L}). Two types of linkers for Man were used with a 3EO unit (short linker denoted as “S” in the name) or 2 × 3EO units (long linker, denoted as “L”). Giant GDSs were prepared by the thin-film hydration method of single JGDs.^[21]

The self-assembly of JGD-1_{Man} and JGD-2_{Man} resulted in the formation of predominantly unilamellar vesicles (Figure S1a, b) while the dilution of Man in the dendrimers resulted in more complex morphologies (Figure 1b, c, and S1). Cryogenic field emission scanning electron microscopy (cryo-FESEM) of cryogenically fractured vesicles and confocal laser scanning microscopy (CLSM) of vesicle dispersion demonstrated the internal onion-like structure of GDS assembled from JGD(8/1_{Man}^{2S}) (Figure 1b, c). Analogously, onion-like GDS were observed for JGD(3/1_{Man}), and 8/1 series, while bicontinuous phases (cubosome and sponge, L₃) were found for JGD(6/1_{Man}) (Figure S1).^[13c,22] Multilamellar vesicles are thermodynamically more favored compared to unilamellar^[21] and are the majoritarian vesicle morphology in this work. Figure 1d depicts a topography image by AFM of an onion vesicle assembled from JGD(8/1_{Man}^{2S}) deposited on mica. A dispersion of giant GDSs was drop cast on the surface of mica and allowed to dry at ambient conditions ($T = 25^\circ\text{C}$, relative humidity (RH) $\approx 25\text{--}30\%$) for at least 3 h to allow partial water evaporation. Such gentle drying conditions allowed us to obtain flattened GDSs with clearly distinguishable bilayers. The presence of well-defined

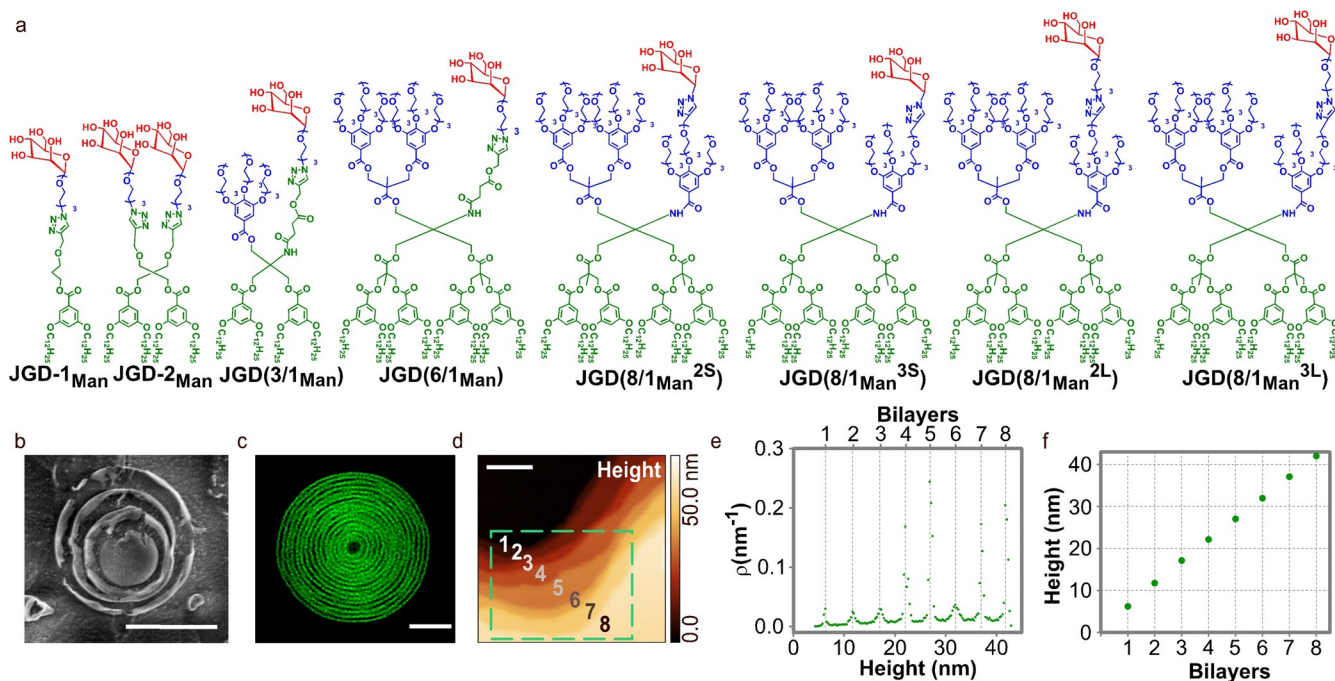


Figure 1. a) Molecular structures of JGDs indicating the nomenclature. GDSs from JGD(8/1_{Man}^{2S}) studied by b) cryo-FESEM of fractured vesicles, c) confocal laser scanning microscopy (CLSM) of BODIPY-labelled bilayers and d) AFM height image of flattened vesicles with at least eight bilayers, (e) height distribution profile of bilayers in the area indicated by green dotted rectangle in (d), and (f) plot indicating the average thickness of bilayers (5.3 nm). Scale bars are 5 μm for (b and c) and 500 nm for (d).

bilayers indicates the presence of associated water on the bilayer surface that does not allow the amphiphiles to rearrange the hydrophobic dendrons toward air. The height distribution profile of a GDS from JGD(8/1_{Man}^{2S}) (Figure 1 d–f) demonstrates the presence of at least eight bilayers with an average thickness of 5.3 nm (Figure 1 e, f).

Structural Analysis of Glycan Nanoarrays at the Surface of GDSs

Previously we reported that sugar-binding ConA exhibits higher aggregation activity toward monodisperse onion-like multilamellar GDSs with a decreased surface density of Man.^[13c] This study indicated a clear impact of Man density, sequence, and spacer length on the biological activity of the sugar to ConA.^[13c] However, the question of whether and how the spatial organization of glycans affects the protein binding remains unclear. In order to tackle this question, we assessed the morphology of the bilayers of the GDSs by a structural analysis methodology using AFM images and their FFT along with complementary molecular modeling as previously described.^[16a,18] This methodology reveals the complex hierarchical self-organization of sugar moieties in the studied molecules. The GDSs formed by JGD-1_{Man}, JGD-2_{Man}, and JGD(8/1_{Man}^{3S}) displayed smooth continuous membranes (Figure 2 d and S2b, e, n). On the other hand, the GDSs from JGD(3/1_{Man}), JGD(8/1_{Man}^{2S}), and JGD(8/1_{Man}^{3L}) exhibited hierarchical lamellar morphologies (Figure 2 a, e, and S2h, k, t). A more complex hexagonal periodic nanoarray was observed exclusively in the membranes of GDSs from JGD(8/1_{Man}^{2L}) (Figure 2 b and S2q). The presence of the nanoarrays

was observed both in the phase and height images. In phase, the domains interact more strongly with the cantilever, which suggests that Man is present and capable of more interactions compared to 3EO. Moreover, the height images demonstrated the difference in height of ≈ 0.5 nm between Man and 3EO phase segregated in nanoarrays proving the presence of Man on the bilayer (Figure S3). No membrane studies were performed for JGD(6/1_{Man}) since this JGD assembles into bicontinuous phases including glycodendrimer-cubosomes.^[13c]

The observed periodic nanoarrays have been found on lipid bilayers such as the highly organized *stratum corneum*^[23] in the skin and have been postulated as necessary for the existence of raft domains. The latter has already been proven in raft mimics.^[5f,24] The nanoarrays are thought to form because they represent the most favorable arrangement of the membrane components. Recently we demonstrated the formation of similar arrays when the sugars were Lac and oligo(Man).^[16a,18] Increasing the length of the sugar resulted not only in an increase in membrane thickness but also in the periodicity of the nanoarray.^[16a,18] Since all dendrimers have the same hydrophobic dendrons, the factors involved in the nanoarray formation should be related to the sugar groups, possibly including dipolar and hydrogen bond interactions, rotational entropy of the sugar headgroup, and molecular shape.^[5f] Molecular modeling (Figure 2 c, f) suggests that JGDs may adopt geometries that would allow Man units to maximize their interactions. JGD-1_{Man} and JGD-2_{Man} achieved this without any segregation resulting in homogeneous membranes. On the other hand, dilution of the sugar with only three 3EO oligomers (JGD(3/1_{Man})) was enough to direct

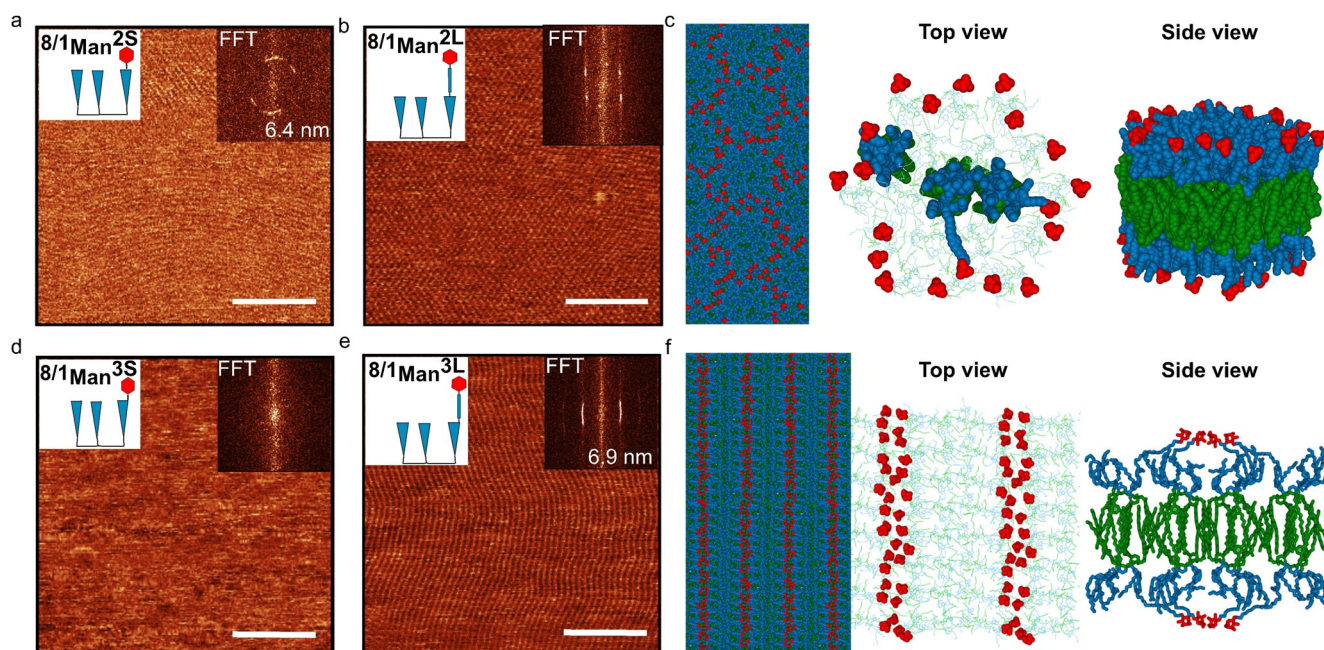


Figure 2. AFM phase images of GDSs formed from a) JGD ($8/1_{\text{Man}}^{2\text{S}}$), b) JGD ($8/1_{\text{Man}}^{2\text{L}}$), d) JGD ($8/1_{\text{Man}}^{3\text{S}}$) and e) JGD ($8/1_{\text{Man}}^{3\text{L}}$) show self-organization of Man moieties on the leaflets of onion-type GDS and its morphology depends on the position and length of the sugar. Models of nanoarrays for GDSs. c) Model of the hexagonal nanoarray (left) of corresponding AFM image (b) for JGD($8/1_{\text{Man}}^{2\text{L}}$). Top view of the bilayer model with all Man moieties and 3 highlighted JGD($8/1_{\text{Man}}^{2\text{L}}$) and side view of a region of the bilayer of the same JGD (right). f) Model of the lamellar nanoarray (left) of corresponding AFM image e) for JGD($8/1_{\text{Man}}^{3\text{L}}$). Top view of the bilayer model with all Man moieties and side view of a region of the bilayer of JGD($8/1_{\text{Man}}^{3\text{L}}$) (right). Scale bars are 100 nm.

the formation of the lamellar pattern on the GDS membranes (Figure 3a and S2h).

To access the effect of the type of sugar we studied nanoarrays on GDSs assembled from JGDs having the same molecular topology and hydrophobic dendrons as in JGD($3/1_{\text{Man}}$), but varying the sugar moiety; galactose (Gal), a monosaccharide, and Lac, a disaccharide (Figure 3). Both monosaccharide-based GDSs (JGD($3/1_{\text{Man}}$), JGD($3/1_{\text{Gal}}$)) have membranes with the same thickness and displayed lamellar morphologies with the same periodicity, 6.6 nm. On the other hand, increasing the length of the sugar to Lac resulted in an increase in membrane thickness and of lamellar spacing (7.0 nm, Figure 3c) similarly to a recent observation for oligo(Man)-sequence defined JGDs.^[16a] This experiment demonstrates that the length of the sugars plays a key role in the membrane thickness, nanoarray assembly, and its lattice parameters.

The dilution of Man with eight 3EO led to the formation of lamellar nanoarrays when the Man residue was linked to the second position in the gallic amide, JGD($8/1_{\text{Man}}^{2\text{S}}$) (Figure 2a and S2k). Surprisingly, placing the Man in the third position, JGD($8/1_{\text{Man}}^{3\text{S}}$), did not show any pattern (Figure 2d, and S2n) despite displaying high glycan activity to ConA as demonstrated by previous agglutination experiments of GDSs.^[13c] Furthermore, replacing Man for Lac in the dendrimers led to lamellar nanoarrays independently of the position of the sugar on the hydrophilic dendron (JGD($8/1_{\text{Lac}}^{2\text{S}}$) and JGD($8/1_{\text{Lac}}^{3\text{S}}$)).^[18] We hypothesized that the 3S (outer-most) position and shorter length of the monosaccharide Man may impede the observation of the lamellar array

under the condition in which AFM was carried out. Conceivably, at ambient conditions, the amount of associated water to bilayers of flattened GDSs formed from JGD($8/1_{\text{Man}}^{3\text{S}}$) may not be enough to maintain the interactions between short Man moieties supporting the nanoarray as it would be in aqueous media. Compared to JGD($8/1_{\text{Lac}}^{3\text{S}}$), in JGD($8/1_{\text{Man}}^{3\text{S}}$) the hydrophilic interactions between sugars that drive the nanoarray formation are presumably weaker and thus more sensitive to the humidity conditions during AFM imaging. To evaluate the role of relative humidity in the evolution and stability of the nanoarrays on GDSs formed from JGD($8/1_{\text{Man}}^{3\text{S}}$) we performed AFM in a humidity-controlled chamber which enabled to gradually vary the humidity while scanning. Firstly, an overview AFM scan was performed at ambient humidity (RH = 25 %) to select a bilayer for continuous high-resolution scanning. No nanoarrays could be detected at RH = 25 % (Figure 4a and S4a). Subsequently, the humidity inside the AFM chamber was slowly raised, while we continued scanning the same area. A weak lamellar nanoarray could be identified in the phase images already at the range of RH = 38–45 % using FFT (Figure 4b). The nanoarray becomes clearer and the lamellar periodicity gradually increased from 7.4 to 8.3 nm by increasing the RH to 45, 60, 70, and 75 % (Figure 4c, d, e and S4a). The increase in the periodicity of the lamella suggests that hydrophilic interactions played a major role in surface nanoorganization. It was not possible to perform AFM scans at RH beyond 75 % due to water condensation and strong capillary forces.^[25] Subsequently, the RH was decreased resulting in a continuous weakening of the lamellar pattern

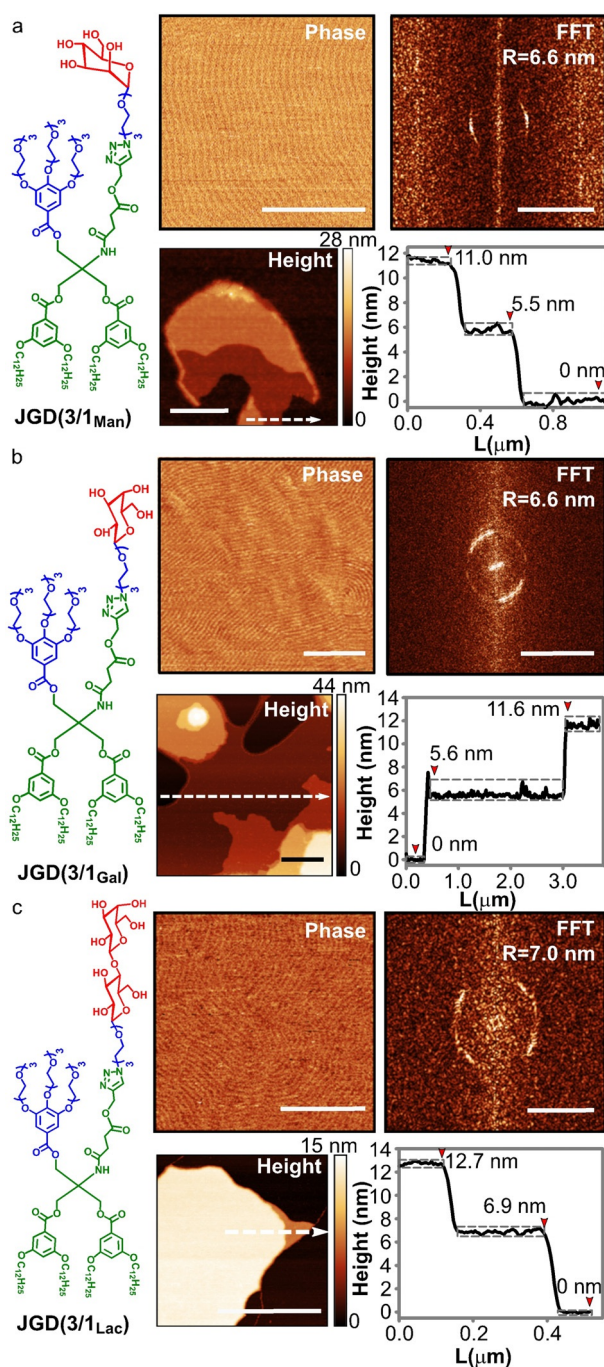


Figure 3. AFM images of GDSs formed from JGDs bearing monosaccharides a) Man and b) Gal and disaccharide c) Lac. These images show that the analogous molecular architecture of JGDs allows the formation of lamellar morphology independent of the type of saccharide, but the type of saccharide influences the thickness of the bilayer (height profiles from the place indicated by white arrow) and lattice parameter (FFTs). Scale bars for phase, FFT, and height images are 100 nm, $400 \mu\text{m}^{-1}$, and 1 μm , respectively.

and reduction of its periodicity from 8.3 nm at RH = 75 % to 6.9 nm at RH = 30 %. Further decreasing the RH to 25 % completely erased the nanoarray. We performed several cycles of humidifying (75 %) and drying (25 %) the AFM chamber whereby we could observe the reversible appear-

ance and disappearance of Man lamellar pattern on bilayers of GDSs formed from JGD(8/1_{Man}^{3S}) (Figure S4a). Decreasing humidity below 20 % broke the bilayer structure resulting in the exposure of hydrophobic dendrons to air, forming a drop-like aggregate on the surface of mica (Figure S5). This experiment demonstrates that the presence of associated water is a *sine qua non* condition for the bilayer and nanoarray observation by AFM.

Furthermore, we examined the effect of the length of the linker on the nanoarray formation. In our previous report, the increase in the length of the linker for JGD(8/1_{Lac}^{2L}) led to the formation of highly ordered hexagonal nanoarrays.^[18] Changing Lac for the shorter Man in JGD(8/1_{Man}^{2L}), also led to hexagonal arrays (Figure 2b). However, while the FFT of JGD(8/1_{Lac}^{2L}) presents up to third-order peaks, only first-order peaks were observed on JGD(8/1_{Man}^{2L}) GDSs (Figure 2b). The relatively shorter range of order suggests that the interactions driving the nanoarrays are weaker for the shorter sugar. Linking the sugar to position 3 in JGD(8/1_{Man}^{3L}) prevented the formation of hexagonal arrays even at increased humidity (Figure 2e and S4b). Conversely, a lamellar structure with longer periodicity than those from JGD(8/1_{Man}^{2S}) or JGD(8/1_{Lac}^{3S}) was observed.^[18] The increase in the lattice parameter is well in line with the increasing length of the linker in JGD(8/1_{Man}^{3L}). Thus, the type of morphology and lattice parameters can be programmed in the type of sugar and length of the linker in a sequence-defined library of JGDs.

Biological Activity of Glycan Nanoarrays

The affinity constants between ConA and Man of the different GDSs were determined using a SPR binding assay. We formed mimics of the membranes by drop-casting a solution of each of the JGDs (0.1 mg mL^{-1}) in THF on the gold-coated SPR sensor slides. The solvent was dried and the samples were annealed at 60 °C to form perfect JGD bilayers on the SPR sensor. The presence of the nanoarrays on gold was confirmed by AFM (Figure S8). The binding of ConA ($50 \mu\text{g mL}^{-1}$, 46 nM in HEPES) was followed by measuring the shift in the angle of resonance of the plasmon at $\lambda_{\text{res}} = 670 \text{ nm}$ to generate the kinetic adsorption curves using a weighted centroid (Figure 5a and S6). Control experiments were performed to confirm that the binding of ConA to the deposited bilayers was mediated by specific interactions with Man and not by unspecific binding. Negligible unspecific binding of ConA was observed on identical bilayers in which Man residues were exchanged for Lac, while no adsorption of a dummy protein (bovine serum albumin) could be detected on bilayer containing Man (Figure S9a).

The binding was modeled as surface coverage ($\theta(t)$) based on the binding-dissociation kinetics following a Langmuir-like adsorption equation:^[26]

$$\frac{d\theta}{dt} = k_a c_0 a (1 - \theta) - k_d \theta \quad (1)$$

where k_a , k_d , c_0 , and a are a kinetic constant of association,

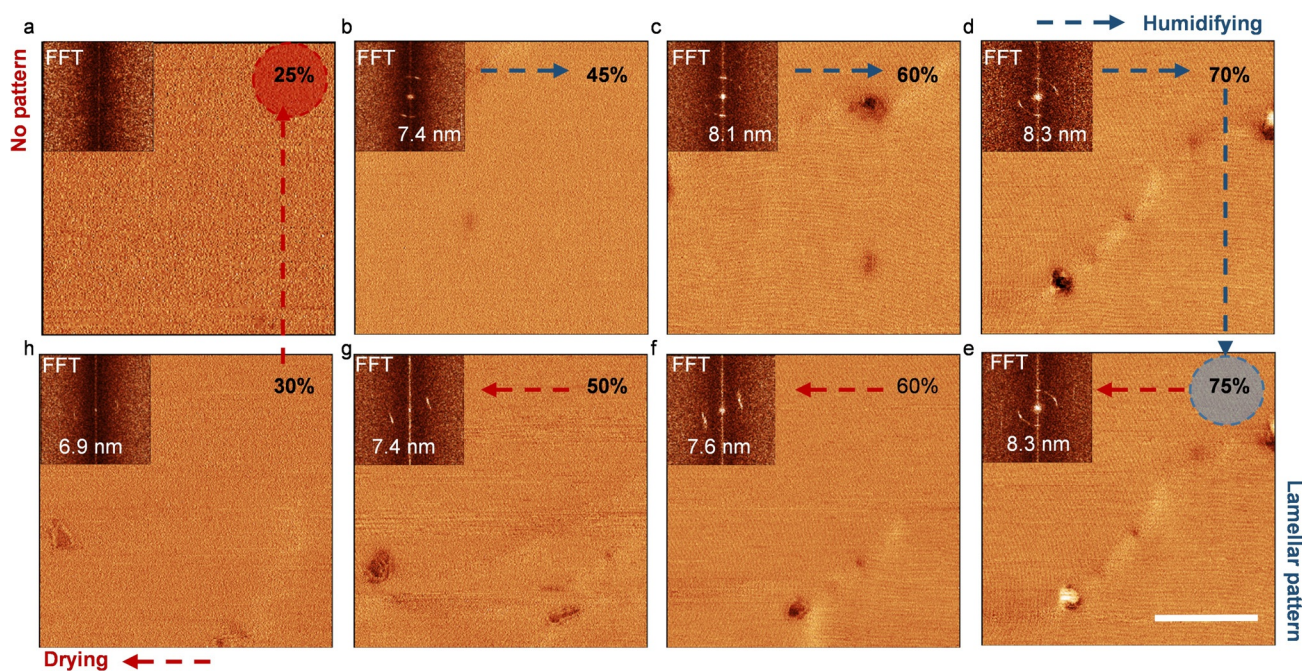


Figure 4. Effect of RH on the nanoarray formation. AFM phase images of GDSs formed from JGD (8/1_{Man}³⁵) measured during humidification: a) 25%, b) 45%, c) 60%, d) 70%, e) 75% RH and drying: f) 60%, g) 50%, h) 30%, and a) 25% of AFM chamber. Scale bar is 200 nm.

dissociation, the concentration of ConA, and a factor to account for the dilution of Man on the GDSs interfaces (refer to SI for the description of the fitting procedure).^[26b] The thermodynamic constant of association was obtained as $K = k_a/k_d$. The unstructured JGD-1_{Man} and JGD-2_{Man} interfaces displayed K of 9.5×10^4 and $5.9 \times 10^4 \text{ M}^{-1}$, respectively (Figure 5b and Table S1). On the other hand, about a ten-fold increase was observed for all the other JGDs that present nanoarrays (Figure 5b and Table S1). Remarkably, such an increase was also observed when the Man residue was directly linked by a triazole, in line with previous works showing no influence of the latter.^[27] Two possible scenarios may cause this drastic change in the K ; the dilution reduces the effect of steric hindrance on the glycans or the nanoarray results in a new effective ligand. It is important to note that despite the overall decrease in the interfacial concentration of Man, the formation of nanoarrays results in Man clusters where the glycan residues may be closer, actually increasing the steric hindrance for bind ConA. Moreover, in a previous study, K was determined for liposomes formed by synthetic Man-decorated glycolipids diluted by phosphatidylcholine in various molar ratios.^[28] Remarkably, only poor binding was observed when the content of Man-decorated glycolipids was below 5% while binding increased thereafter with increasing densities of Man, resulting in K for 10% dilution very similar ($2.7 \times 10^4 \text{ M}^{-1}$) to the ones observed by unstructured 100% GDSs (JGD-1_{Man} and JGD-2_{Man}). This suggests that steric hindrance did not play a major role. Examination of the kinetic constants of association (k_a) followed the same trend, the GDSs having nanoarrays had k_a at least one order of magnitude higher than the high-density unstructured GDSs from (JGD-1_{Man} and JGD-2_{Man}) (Figure 5c, S7, and Table S1). Conversely, all GDSs displayed similar k_d (Figure 5c and Table S1). These findings prove that the binding of the ConA

is favored by the nanoarray formation.

Presumably, the combination of preorganization of the glycans would result in a local increase in the concentration of Man and a concomitant increase in the microscopic avidity constant via multivalent interactions. Similar effects have been shown for multivalent trimannoside analogs interacting with ConA, for which the enhancement of avidity was demonstrated to be governed by a greater positive entropy contribution.^[29] Moreover, the increased avidity might be associated with a better match between the binding sites of ConA (about 8 nm apart) and separation of glycan cluster the nanoarrays on the surface of GDSs.^[28,30] Conversely, such type of multivalent interactions are not expected to have a strong effect in the dissociation well in line with the observation of almost invariant k_d among all GDSs studied. Multivalent interactions, like the ones observed here, are exploited in biology to translate weak bonds into strong binding.^[19c-e,31] But Frenkel recognized the importance of clustering of receptors in these type of multivalent interactions and coined the concept of superselectivity.^[32] The clustering of receptors results in a strong effect in the combinatorial entropy, which ultimately leads to systems that display very strong binding only above a certain threshold of receptors.^[19c,32] Thus, understanding these types of interactions may provide design principles to target cancer cells that overexpress receptors, which are also exhibited in healthy ones, and shed light on various mechanisms of cell communication and transmembrane trafficking.

Conclusion

This work elucidated the mechanism via which sequence-defined GDSs displayed enhanced glycan reactivity. The

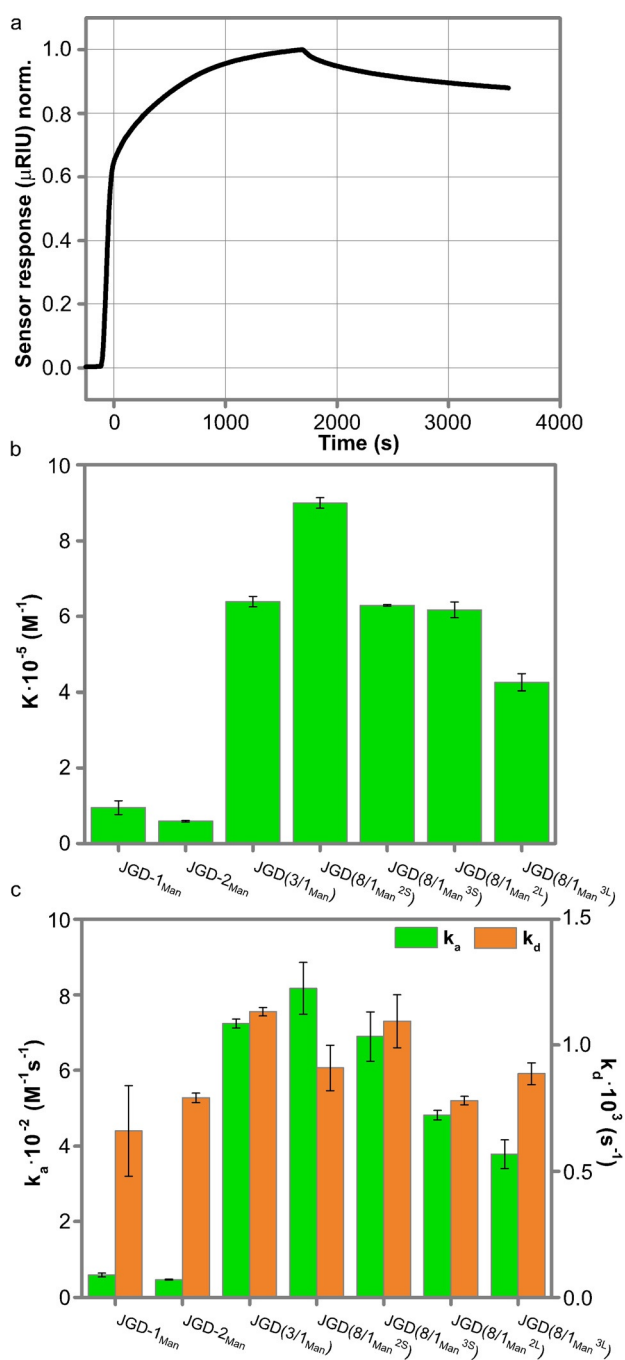


Figure 5. a) Signal intensity normalized SPR sensogram of ConA binding on JGD(3/1_{Man}) functionalized gold surfaces obtained at 670 nm. b) The thermodynamic constant and c) kinetic constants of association and dissociation of the ConA association to Man moieties of JGDs' functionalized gold surfaces.

supramolecular organization at the membrane interface was assessed using AFM. The GDSs assembled from JGD-1_{Man} and JGD-2_{Man} displayed very compact packing of the Man units into homogeneous membranes. However, dilution of the Man units with 3EO groups resulted in the formation of lamellar and hexagonal nanoarrays in a similar fashion as those previously observed for Lac. Molecular modeling suggested that these morphologies were driven by weak

forces among the glycan moieties which clustered to maximize their interactions. It was supported by the observation that the length of the sugars, and thus the strength of the interactions, played a central role in the type of nanoarray and its stability. Similar patterns could be obtained when Man was exchanged with Gal, however, substituting Man for Lac, a disaccharide, resulted in an increase in the periodicity. Furthermore, the Man nanoarrays were more sensitive to atmospheric RH than those observed for Lac-GDSs as demonstrated by AFM studies under controlled humidity. Remarkably, the Man nanoarrays could be erased and reformed by reducing and increasing the humidity in a cyclic manner. This observation revealed that hydrophilic interactions involving glycan and water were essential in the formation of the nanoarrays.

The binding kinetics of ConA to Man residues on the membranes demonstrated a ten-fold increase in the thermodynamic constant of association when the Man residues were diluted, while similar dilutions of the Man residues in liposomes did not result in a similar increase in the binding strength. This observation proved that the reduction of steric hindrance was not the cause of the enhanced reactivity, but the presence of the nanoarrays. The examination of the kinetic constants further supported this conclusion. The k_a was at least an order of magnitude higher for those membranes displaying nano-organized sugars, while the k_d remained invariant, indicating that multivalent interactions originating from the nanoarrays are part of the observed binding.

This study demonstrates that the complexity of the interactions between proteins and sugars that are part of the glycocalyx is not only controlled by the type of sugar, degree of polymerization, and branching but also by the two-dimensional organization at the membrane. Such principles are the basis of the raft domain theory and remain to be unveiled. Understanding how to program binding on the nanoarrays will undoubtedly result in a leap forward in the understating of various cellular processes, the pathogenicity of bacteria and viruses and for the design of novel therapeutics.

Acknowledgements

The authors acknowledge the support of H2020-NMBP-TR-IND-2018, EVPRO (Development of Extracellular Vesicles loaded hydrogel coatings with immunomodulatory activity for Promoted Regenerative Osseointegration of revision endoprosthesis) grant 814495-2 (to C.R.-E., N.Y.K.), financial support by the National Science Foundation (DMR-1807127 (to V.P.), DMR-1720530 (to V.P.)), and the P. Roy Vagelos Chair at Penn (to V.P.). Alexander von Humboldt Foundation (N.Y.K. and V.P.) is gratefully acknowledged. M.L.K. thanks HRH Sheikh Saud for the award of a Sheikh Saqr Research Fellowship. This work was also partially performed at the Center for Chemical Polymer Technology CPT, which was supported by the EU and the federal state of North Rhine-Westphalia (grant EFRE 30 00 883 02). The authors thank Stephan Rütten for help with Cryo-FESEM preparation.

Open access funding enabled and organized by Projekt DEAL.

Conflict of interest

The authors declare no conflict of interest.

Keywords: glycan nanoarray · glycolyx · Janus dendrimers · raft domains · synthetic cell

- [1] H. J. Gabius, *Biosystems* **2018**, *164*, 102–111.
- [2] a) T. Harder, P. Scheffele, P. Verkade, K. Simons, *J. Cell Biol.* **1998**, *141*, 929–942; b) D. Lingwood, K. Simons, *Science* **2010**, *327*, 46–50; c) K. Simons, E. Ikonen, *Nature* **1997**, *387*, 569–572; d) I. Levental, H. Y. Wang, *J. Lipid Res.* **2020**, *61*, 592–594.
- [3] C. R. Shurer, J. C. Kuo, L. M. Roberts, J. G. Gandhi, M. J. Colville, T. A. Enoki, H. Pan, J. Su, J. M. Noble, M. J. Hollander, J. P. O'Donnell, R. Yin, K. Pedram, L. Mockl, L. F. Kourkoutis, W. E. Moerner, C. R. Bertozzi, G. W. Feigenson, H. L. Reesink, M. J. Paszek, *Cell* **2019**, *177*, 1757–1770.
- [4] a) M. A. Tortorici, A. C. Walls, Y. Lang, C. Wang, Z. Li, D. Koerhuis, G. J. Boons, B. J. Bosch, F. A. Rey, R. J. de Groot, D. Velesler, *Nat. Struct. Mol. Biol.* **2019**, *26*, 481–489; b) S. C. Purcell, K. Godula, *Interface Focus* **2019**, *9*, 20180080; c) M. Cohen, A. Varki in *International Review of Cell and Molecular Biology*, Vol. 308 (Ed.: K. W. Jeon), Academic Press, New York, **2014**, pp. 75–125; d) S. A. Springer, P. Gagneux, *J. Biol. Chem.* **2013**, *288*, 6904–6911; e) M. Koehler, M. Delguste, C. Sieben, L. Gillet, D. Alsteens, *Annu. Rev. Virol.* **2020**, *7*, 143–165.
- [5] a) J. A. Virtanen, M. Ruonala, M. Vauhkonen, P. Somerharju, *Biochemistry* **1995**, *34*, 11568–11581; b) P. J. Somerharju, J. A. Virtanen, K. K. Eklund, P. Vainio, P. K. J. Kinnunen, *Biochemistry* **1985**, *24*, 2773–2781; c) P. L. Chong, *Proc. Natl. Acad. Sci. USA* **1994**, *91*, 10069–10073; d) D. Tang, P. L. G. Chong, *Biophys. J.* **1992**, *63*, 903–910; e) T. R. Weikl, R. Lipowsky in *Advances in Planar Lipid Bilayers and Liposomes*, Vol. 5 (Ed.: A. L. Liu), Elsevier, Amsterdam, **2006**, pp. 63–127; f) P. Somerharju, J. A. Virtanen, K. H. Cheng, M. Hermansson, *Biochim. Biophys. Acta Biomembr.* **2009**, *1788*, 12–23.
- [6] a) T. Eierhoff, B. Bastian, R. Thuenauer, J. Madl, A. Audfray, S. Aigal, S. Juillot, G. E. Rydell, S. Muller, S. de Bentzmann, A. Imberty, C. Fleck, W. Romer, *Proc. Natl. Acad. Sci. USA* **2014**, *111*, 12895–12900; b) S. Aigal, J. Claudinon, W. Romer, *Biochim. Biophys. Acta Mol. Cell Res.* **2015**, *1853*, 858–871; c) S. Villringer, J. Madl, T. Sych, C. Manner, A. Imberty, W. Romer, *Sci. Rep.* **2018**, *8*, 1932; d) D. M. Ratner, E. W. Adams, M. D. Disney, P. H. Seeberger, *ChemBioChem* **2004**, *5*, 1375–1383; e) M. L. Hecht, P. Stallforth, D. V. Silva, A. Adibekian, P. H. Seeberger, *Curr. Opin. Chem. Biol.* **2009**, *13*, 354–359; f) O. J. Plante, E. R. Palmacci, P. H. Seeberger, *Science* **2001**, *291*, 1523–1527; g) A. Varki, *Glycobiology* **1993**, *3*, 97–130; h) J. C. Paulson, *Trends Biochem. Sci.* **1989**, *14*, 272–276.
- [7] a) L. Möckl, K. Pedram, A. R. Roy, V. Krishnan, A. K. Gustavsson, O. Dorigo, C. R. Bertozzi, W. E. Moerner, *Dev. Cell* **2019**, *50*, 57–72; b) M. J. Paszek, C. C. DuFort, O. Rossier, R. Bainer, J. K. Mouw, K. Godula, J. E. Hudak, J. N. Lakin, A. C. Wijekoon, L. Cassereau, M. G. Rubashkin, M. J. Magbana, K. S. Thorn, M. W. Davidson, H. S. Rugo, J. W. Park, D. A. Hammer, G. Giannone, C. R. Bertozzi, V. M. Weaver, *Nature* **2014**, *511*, 319–325.
- [8] a) R. Omidvar, W. Romer, *Interface Focus* **2019**, *9*, 20180084; b) N. Stühr-Hansen, J. Madl, S. Villringer, U. Aili, W. Romer, O. Blixt, *ChemBioChem* **2016**, *17*, 1403–1406.
- [9] I. Levental, K. R. Levental, F. A. Heberle, *Trends Cell Biol.* **2020**, *30*, 341–353.
- [10] a) S. Munro, *Cell* **2003**, *115*, 377–388; b) S. Sadeghi, M. Muller, R. L. Vink, *Biophys. J.* **2014**, *107*, 1591–1600.
- [11] a) D. E. Discher, A. Eisenberg, *Science* **2002**, *297*, 967–973; b) H. Bermúdez, A. K. Brannan, D. A. Hammer, F. S. Bates, D. E. Discher, *Macromolecules* **2002**, *35*, 8203–8208; c) H. Bermudez, D. A. Hammer, D. E. Discher, *Langmuir* **2004**, *20*, 540–543; d) F. Itel, M. Chami, A. Najer, S. Lörcher, D. Wu, I. A. Dinu, W. Meier, *Macromolecules* **2014**, *47*, 7588–7596.
- [12] V. Percec, D. A. Wilson, P. Leowanawat, C. J. Wilson, A. D. Hughes, M. S. Kaucher, D. A. Hammer, D. H. Levine, A. J. Kim, F. S. Bates, K. P. Davis, T. P. Lodge, M. L. Klein, R. H. DeVane, E. Aqad, B. M. Rosen, A. O. Argintaru, M. J. Sienkowska, K. Rissanen, S. Nummelin, J. Ropponen, *Science* **2010**, *328*, 1009–1014.
- [13] a) V. Percec, P. Leowanawat, H. J. Sun, O. Kulikov, C. D. Nusbaum, T. M. Tran, A. Bertin, D. A. Wilson, M. Peterca, S. Zhang, N. P. Kamat, K. Vargo, D. Moock, E. D. Johnston, D. A. Hammer, D. J. Pochan, Y. Chen, Y. M. Chabre, T. C. Shiao, M. Bergeron-Brlek, S. Andre, R. Roy, H. J. Gabius, P. A. Heiney, *J. Am. Chem. Soc.* **2013**, *135*, 9055–9077; b) Q. Xiao, S. S. Yadavalli, S. Zhang, S. E. Sherman, E. Fiorin, L. da Silva, D. A. Wilson, D. A. Hammer, S. Andre, H. J. Gabius, M. L. Klein, M. Goulian, V. Percec, *Proc. Natl. Acad. Sci. USA* **2016**, *113*, E1134–E1141; c) Q. Xiao, S. Zhang, Z. Wang, S. E. Sherman, R. O. Moussodia, M. Peterca, A. Muncan, D. R. Williams, D. A. Hammer, S. Vertesy, S. Andre, H. J. Gabius, M. L. Klein, V. Percec, *Proc. Natl. Acad. Sci. USA* **2016**, *113*, 1162–1167.
- [14] a) N. Y. Kostina, K. Rahimi, Q. Xiao, T. Haraszti, S. Dedisch, J. P. Spatz, U. Schwaneberg, M. L. Klein, V. Percec, M. Moller, C. Rodriguez-Emmenegger, *Nano Lett.* **2019**, *19*, 5732–5738; b) M. Peterca, V. Percec, P. Leowanawat, A. Bertin, *J. Am. Chem. Soc.* **2011**, *133*, 20507–20520.
- [15] N. Y. Kostina, A. M. Wagner, T. Haraszti, K. Rahimi, Q. Xiao, M. L. Klein, V. Percec, C. Rodriguez-Emmenegger, *Soft Matter* **2021**, *17*, 254–267.
- [16] a) Q. Xiao, M. Delbianco, S. E. Sherman, A. M. Reveron Perez, P. Bharate, A. Pardo-Vargas, C. Rodriguez-Emmenegger, N. Y. Kostina, K. Rahimi, D. Soder, M. Moller, M. L. Klein, P. H. Seeberger, V. Percec, *Proc. Natl. Acad. Sci. USA* **2020**, *117*, 11931–11939; b) S. Zhang, R. O. Moussodia, S. Vertesy, S. Andre, M. L. Klein, H. J. Gabius, V. Percec, *Proc. Natl. Acad. Sci. USA* **2015**, *112*, 5585–5590.
- [17] S. Morandat, S. Azouzi, E. Beauvais, A. Mastouri, K. El Kirat, *Anal. Bioanal. Chem.* **2013**, *405*, 1445–1461.
- [18] C. Rodriguez-Emmenegger, Q. Xiao, N. Y. Kostina, S. E. Sherman, K. Rahimi, B. E. Partridge, S. Li, D. Sahoo, A. M. Reveron Perez, I. Buzzacchera, H. Han, M. Kerzner, I. Malhotra, M. Moller, C. J. Wilson, M. C. Good, M. Goulian, T. Baumgart, M. L. Klein, V. Percec, *Proc. Natl. Acad. Sci. USA* **2019**, *116*, 5376–5382.
- [19] a) F. J. Martinez-Veracoechea, D. Frenkel, *Proc. Natl. Acad. Sci. USA* **2011**, *108*, 10963–10968; b) C. Fasting, C. A. Schalley, M. Weber, O. Seitz, S. Hecht, B. Kokschi, J. Dornedde, C. Graf, E. W. Knapp, R. Haag, *Angew. Chem. Int. Ed.* **2012**, *51*, 10472–10498; *Angew. Chem.* **2012**, *124*, 10622–10650; c) X. Tian, S. Agioletti-Uberti, G. Battaglia, *ChemRxiv* **2018**, <https://doi.org/10.26434/chemrxiv.5647969.v4>; d) L. L. Kiessling, A. C. Lamanna, *Multivalency in Biological Systems*, Vol. 129, Springer, Dordrecht, **2003**; e) M. Mammen, S. K. Choi, G. M. Whitesides, *Angew. Chem. Int. Ed.* **1998**, *37*, 2754–2794; *Angew. Chem.* **1998**, *110*, 2908–2953.
- [20] a) P. I. Hanson, A. Cashikar, *Annu. Rev. Cell Dev. Biol.* **2012**, *28*, 337–362; b) S. Zhang, H. J. Sun, A. D. Hughes, R. O. Mousso-

- dia, A. Bertin, Y. Chen, D. J. Pochan, P. A. Heiney, M. L. Klein, V. Percec, *Proc. Natl. Acad. Sci. USA* **2014**, *111*, 9058–9063.
- [21] D. D. Lasic, *Biochem. J.* **1988**, *256*, 1–11.
- [22] S. E. Wilner, Q. Xiao, Z. T. Graber, S. E. Sherman, V. Percec, T. Baumgart, *Langmuir* **2018**, *34*, 5527–5534.
- [23] J. A. Bouwstra, M. Ponc, *Biochim. Biophys. Acta Biomembr.* **2006**, *1758*, 2080–2095.
- [24] P. L. Chong, F. Liu, M. M. Wang, K. Truong, I. P. Sugar, R. E. Brown, *J. Fluoresc.* **1996**, *6*, 221–230.
- [25] T. Ondarçuhu, L. Fabié in *Surface Tension in Microsystems: Engineering Below the Capillary Length (Microtechnology and MEMS)* (Ed.: P. Lambert), Springer, Berlin, **2013**, pp. 279–305.
- [26] a) I. Langmuir, *J. Am. Chem. Soc.* **1918**, *40*, 1361–1403; b) C. Tamerler, E. E. Oren, M. Duman, E. Venkatasubramanian, M. Sarikaya, *Langmuir* **2006**, *22*, 7712–7718.
- [27] J. Geng, J. Lindqvist, G. Mantovani, G. Chen, C. T. Sayers, G. J. Clarkson, D. M. Haddleton, *QSAR Comb. Sci.* **2007**, *26*, 1220–1228.
- [28] D. A. Mann, M. Kanai, D. J. Maly, L. L. Kiessling, *J. Am. Chem. Soc.* **1998**, *120*, 10575–10582.
- [29] a) T. K. Dam, R. Roy, D. Pagé, C. F. Brewer, *Biochemistry* **2002**, *41*, 1351–1358; b) T. K. Dam, R. Roy, S. K. Das, S. Oscarson, C. F. Brewer, *J. Biol. Chem.* **2000**, *275*, 14223–14230.
- [30] a) L. L. Kiessling, *Bioorg. Med. Chem.* **2018**, *26*, 5229–5238; b) L. L. Kiessling, M. B. Kraft, *Science* **2013**, *341*, 357–358.
- [31] J. D. Badjić, A. Nelson, S. J. Cantrill, W. B. Turnbull, J. F. Stoddart, *Acc. Chem. Res.* **2005**, *38*, 723–732.
- [32] G. V. Dubacheva, T. Curk, D. Frenkel, R. P. Richter, *J. Am. Chem. Soc.* **2019**, *141*, 2577–2588.

Manuscript received: January 17, 2021

Accepted manuscript online: January 25, 2021

Version of record online: March 4, 2021